4D reservoir monitoring using slowness

B. de Cacqueray[(1)], P. Roux[(2)], M. Campillo[(2)].

Introduction

In the last 20 years, a lot of efforts has been done in seismology and geophysics to track and monitor sub-surface property variations such as velocity, fluid pressure or saturation. As recent seismological monitoring algorithms focus mainly on noise records (Brenguier et al. 2008, Hadziioannou et al. 2011), geophysical exploration preferably uses ballistic arrivals recorded between sources and receivers. The latter met a regain of interest with the development of the so-called "4D exploration" or reservoir monitoring, where the monitoring result is spatially localized within the volume of interest.

In 4D monitoring, the two main observables are velocity and amplitude variations. Velocity variations are classically monitored using travel time variations as it can be shown that the dt/t quantity of late arrivals is linked to the dv/v quantity at depth. In parallel, investigations have been done on amplitude variations monitoring as e.g. in oceanography, (Marandet et al. 2011). Today, combined travel time and amplitude variations measures becomes possible (Cotton et al. 2012). In recent years, 4D monitoring showed successful results in seismic prospection with conventional surveys (Barkved et al. 2005) or buried system, and even with passive sources (Forgues et al. 2011).

Among potential difficulties encountered in 4D monitoring, compensation of the near-surface variations is an important issue that may be addressed by the cross-equalization technique (Ross et al. 1996). Considering several stacks of wavelets issued from the same area and acquired at different times, the cross equalization consists in matching the wavelets in both phase and amplitude. This work is made difficult because of the (somewhat large) static fluctuations occurring at the near-surface that potentially hide the variations at depth. It is also biased when several wave arrivals superimpose in the time-gated wavelets. Such method generally relies on stacking CDP (Common-Depth-Point) collections of traces in order to get a non-ambiguous estimation of the useful wavelets. More recently, (Cotton et al 2012) proposes a calendar filtering to remove ghost variations in case of buried sources and/or receivers while (de Cacqueray et al. 2013) proposes a new method using array processing to take into account the ray paths differences and compensate for the near-surface variations.

In this paper, we present an advanced array processing method to measure new observables linked with the velocity variations in 4D monitoring such as the slowness at both the source and the receiver sides.

Double beamforming algorithm

The capability of the Double Beamforming (DBF) technique to separate different wave arrivals was successfully demonstrated in seismology (Weber et al, 1996), underwater acoustics (Roux et al. 2008) or through laboratory scale experiments in a geophysical-like context (de Cacqueray et al, 2011) with 2D source-receiver antennas.

In this last study, the data recorded in a 5 dimensional space $S(t,x_s, y_s\, x_r\, y_r)$, where (x_s,y_s) are the source coordinates and (x_r,y_r) the receiver coordinates, can be projected in a new 5-dimensionnal space $\acute{S}$ $(t,\theta_s,\phi_s,\theta_r,\phi_r)$ in the incidence/azimuth (θ, ϕ) domain of each source-receiver array or better

$\hat{S}(t,u_s,\phi_s,u_r,\phi_r)$ in the slowness (u) /azimuth (ϕ) domain. Indeed, the incidence angle can be derived from the slowness when the local velocity is known according to the relation:

$$u=\sin(\theta)/V$$

With 1D collinear source and receiver antennas, one can consider only slownesses and refer to the 3 dimensional $\hat{S}(t,u_s,u_r)$ (figure 1).

Through the DBF projection, each eigenbeam is represented by an intensity maximum in the $\hat{S}$ matrix that matches an eigenray path in the physical space. By projecting the propagating waves on planar wavefronts, the advantage of the DBF technique is both (a) to enhance signal-to-noise ratio through array gain and (b) to separate and identify the contribution of different wave arrivals (figure 1b). In 4D monitoring, wave separation is essential since it avoids measuring time variations in a window mixing different arrivals with different time variations.

With repetitive records for all the source-receiver pairs over a given period, DBF permits to extract a set of eigen beams from each record. Once identified and matched to a ray path, the corresponding arrival times, slownesses and/or azimuths can be measured and monitored, as demonstrated with experiments at the laboratory scale (de Cacqueray et al. 2012).

Field experiment

The results obtained in 4D monitoring with laboratory data have now to be demonstrated for field environments. There are only few acquisition designs dedicated for simultaneous source and receiver arrays. Nevertheless, the number of receivers and sources on the field is generally high enough so that subsets can be chosen and used as arrays.

The dataset used in this section comes from a field trial set up to monitor steam injection within a reservoir using injection wells. Several lines of receivers and one line of buried sources are buried to permanently monitor the sub-surface variations. We use data already pre-processed so that a significant part of the spurious waves (like surface waves and S-body waves) and spurious arrival time fluctuations have been removed. In the field trial, piezo-sources at 25-m depth emitting in the [5 180] Hz range and hydrophones buried at 9-m depth are used. Due to the in-line positioning, only 1D source-receiver arrays were processed. Figure 2 represents the buried receivers (squares) and the buried sources (circles) and figure 3 represents raw data for one source and one line of 68 receivers.

The field environment is not designed for 4D monitoring using array processing. The subset of sources and receivers selected for DBF has not been optimised for this usage. In particular, the receiver spacing is 16 m while the source spacing is about 80 m. For frequencies above 40 Hz, the planar projection on the source-receiver arrays is unperfect as the far field hypothesis between the two arrays is not respected. Moreover, the poor spatial sampling on the source array may induce spatial alisasing, i.e. strong sidelobes in the beam space.

To fix the first issue, a subset of 15 receivers was selected far enough from the 7 sources (black squares in figure 2). In consequence, the monitored area was shifted to the left compared to the main zone of interest (see ellipses in figure 2). This is a possible drawback as the source line was buried above the area of injection.

For spatial aliasing, the beam projection was computed theoretically using parameters close to the field trial with a constant P-wave velocity of 2000 m/s. It means that the maximum slowness is 0.5 s/km. The

beams are plotted for one body wave reflection with source and receiver incidence of 68° at three different frequencies [figure 4].Apparent slowness ranges from 0.1 to 0.8 s/km. For the reflected wave, aliasing is observed from 20 Hz on source side [fig 4(a)], and from 100 Hz on receiver side [fig. 4(b)]. At 150 Hz, the aliasing appears on receiver side at 0.6 s/km [fig. 4(c)], which is still below the 0.5 s/km limit. At this incidence, the limit is reached at 197 Hz. It means that thanks DBF and providing that no interfering wavefront appears at this arrival time, we are able to separate the P-wave without aliasing up to more than 150Hz. Additionally, when the propagation medium is relatively homogeneous, intensity spots for which the source-receiver slownesses are too different from each other can be ignored. Finally, figure 4(d) represents the reflected wave intensity spot for a full bandwidth ranging from 15 Hz to 150 Hz

Despite the unfavourable configuration to measure the 4D effects induced by the steam injection, having daily records from field trial is rare enough to try to get the maximum benefit of it. In particular, any coherency between arrival time and slowness variations would be an important result.

In figure 3, we observe that for a given wave arrival, the amplitude of the corresponding wavelet varies significantly from one trace to the other. This comes from the attenuation which varies with the offset and the travel time and could lead to biased results after DBF. To avoid such problem, the amplitude of each wavelet is normalised prior to the DBF process.

Results

Results are presented in the slowess domain rather than the angle domain., Several spatially-coherent wavefronts are visible in the raw data (Figure 3). To evaluate the performances of the algorithm, we chose one wave arriving around 428 ms and apply DBF

Figure 5 shows the resulting time/slowness beams on the source-receiver arrays and the corresponding wavelet extracted with DBF for 152 days. To avoid the noise at lower frequencies and to keep a margin vs aliasing, the chosen bandwidth ranges from 35 to 170 Hz. As expected in figure 5(a) and (b), the source and receiver slowness have similar values around 0.35 s/km. In figure 5(c), note that the wavelet is properly extracted from the data. In practice, monitoring the slowness is performed from the time/slowness representation for each day when arrival time variations are measured from the extracted wavelet. Then, 4D monitoring requires the selection of 3 reflections with the following parameters:

Reflection	Arrival time (ms)	Source slowness (s/km)	Receiver slowness (s/km)
Wave 1 – above reservoir	150	0.5	0.5
Wave 2 – at reservoir depth	690	0.141	0.137
Wave 3 – below reservoir	720	0.113	0.113

To measure accurate arrival time variations, each wavelet is cross-correlated after DBF with the wavelet of day 1. The arrival time variations are computed at the maximum of the correlation with second-order interpolation. For slowness, the same cross-correlation and interpolation is performed in the slowness domain at the time of the beam maximum.

Figure 6 shows the results for wave 1 to 3. Figure 6(a), (b) and (c) show minor variations for the reflection above the reservoir. This observation is confirmed for arrival time, source slowness and receiver slowness. For the reflection in the reservoir, the variations are stronger. In particular, the slownesses vary in opposite sense which is consistent with a local velocity change at depth. Additionally, taking into account the sign inversion for the receiver slowness, we observe a good consistency between arrival time variations and slownesses variations. This also true for the wave below the reservoir where significant events after 100 days are noticeable for the three observables.

Independent available information regarding the field mentions steam injection around day 40. This is in agreement with the present observations since the dominant fluctuation starts between days 40 and 60 for the waves 2 and 3 that propagate in or through the reservoir,.

Conclusion

As for laboratory data, DBF appears as a promising tool to separate and identify reflected waves. Due to DBF processing requirement, monitor accurately the 4D target area was not feasible. However, consistant results have been highlighted between source and reception slownesses variations and arrival time variations. Slowness monitoring appears a new way to monitor sub-surface variations, complimentary to amplitude and time variations. The next step would be to set up new monitoring designs on the field with 2D antennas and finer source spatial sampling to optimize the benefit of the DBF processing.

Aknowledgement

We would like to thanks Shell and NAM who kindly lent us the field dataset.

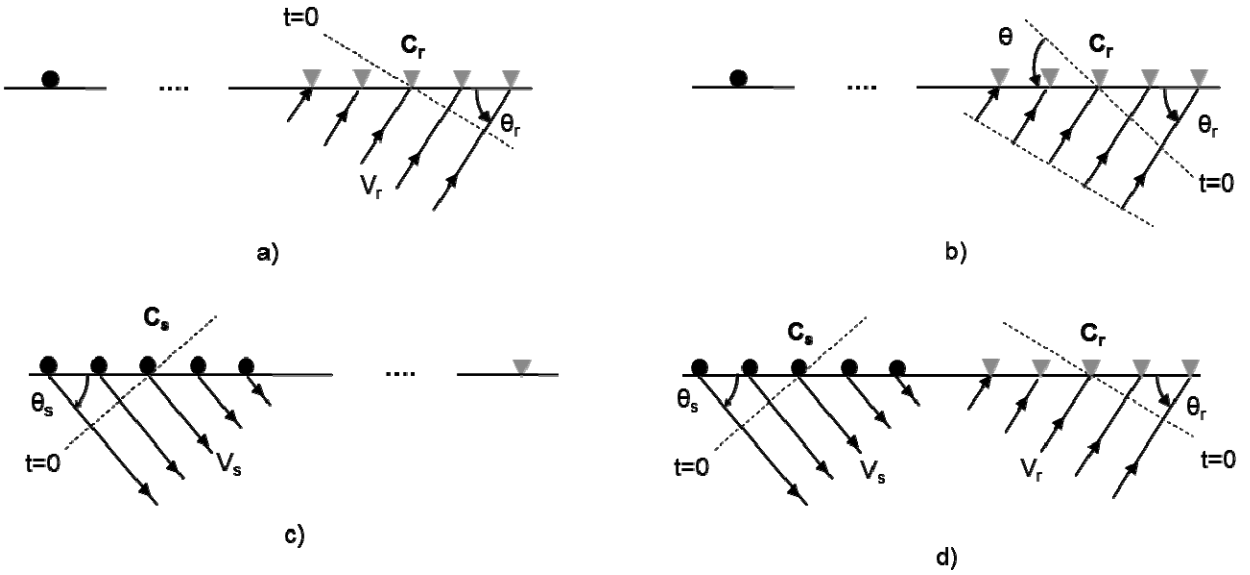

Figure – 1 (a) (black circle) source, (grey triangles) receivers, (C_r) receiver array center, (θ_r arrival angle, (dashed line) in-phase plane for time reference, (V_r) velocity at the receiver array. By projecting the incident wavefronts on plane waves, the beamforming transforms the recorded data on the receiver array from the position domain to the angle domain, in such a way that the wavefield intensity is focused at certain elevation angles (represented by the angle θ_r). According to the relation $u_r = cos\ \theta_r/V_r$, where u_r is the slowness, the beamforming is computed in the slowness domain. (b) Applying relevant delays to each received trace allows scanning complete offset ranges. When $\theta = \theta_r$ the signals from all receivers are in-phase so that the resultant sum present a maximum after summation. (c) (black circles) sources, (grey triangle) receiver, (C_s) receiver array center, (dashed line) in-phase plane for time reference, (V_s) velocity at the source array. According to the reciprocity theorem, beamforming can also be performed on the source array with respect to the reference point C_s. (c) When used simultaneously at the source and receiver arrays, the beamforming process is called double beamforming (DBF). As planar wave fronts are formed at both the source and receiver sides, DBF remains efficient even at short source-receiver distances. DBF provides the selection of waves with respect to their source and receiver slownesses.

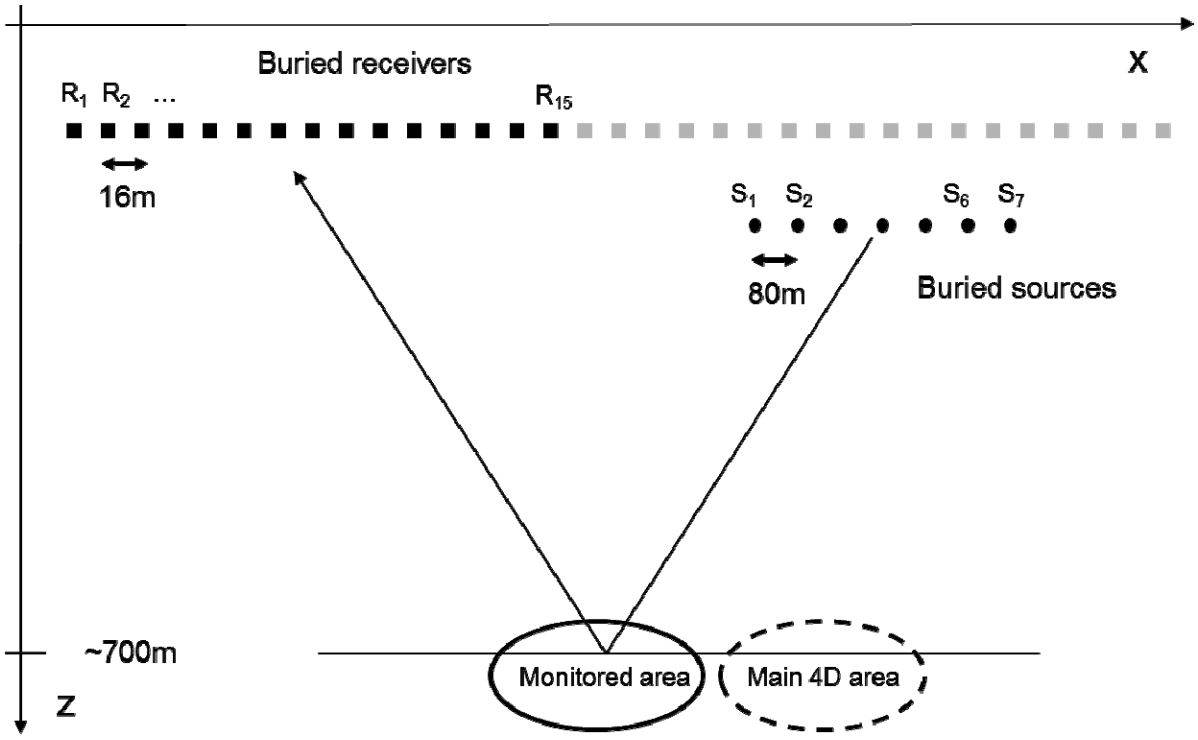

Figure – 2 (squares) buried receivers (circles) buried sources (dash line ellipse) area with main 4D effect (black ellipse) monitored area.

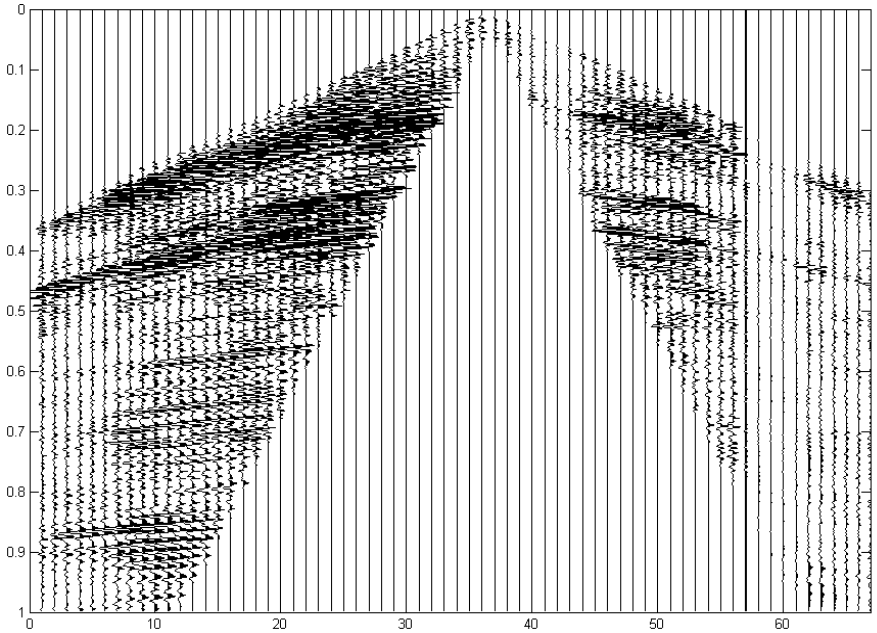

Figure 3 - Record for 68 hydrophons parallel to the source line filtered in the [35 170] Hz band. A sperical divergence correction has been applied to enhance later reflections. We note numerous reflections. The part of traces without signal come from a processing step where S-body wave have been muted.

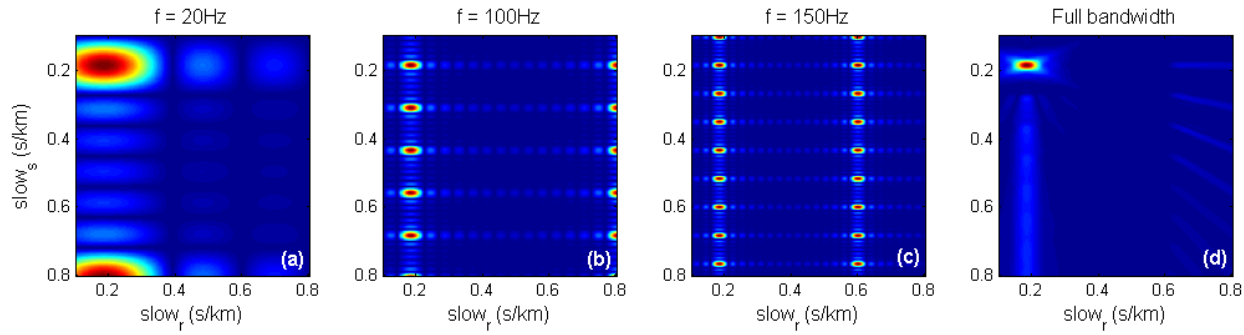

Figure 4 - Aliasing (a)-(c) focal spots at frequencies 20, 100 et 150 Hz for the reflectedwave and (d) resulting spot after summation over the full [15 150] Hz bandwidth.

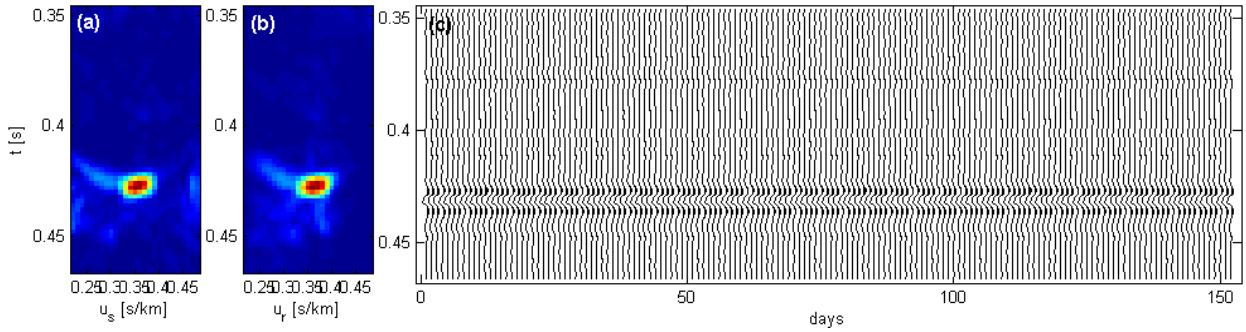

Figure 5 - Wave around 428 ms in the [35 170] Hz frequency band (a) source time/slowness map (b) reception time/slowness map (c) extracted wave for 152 days.

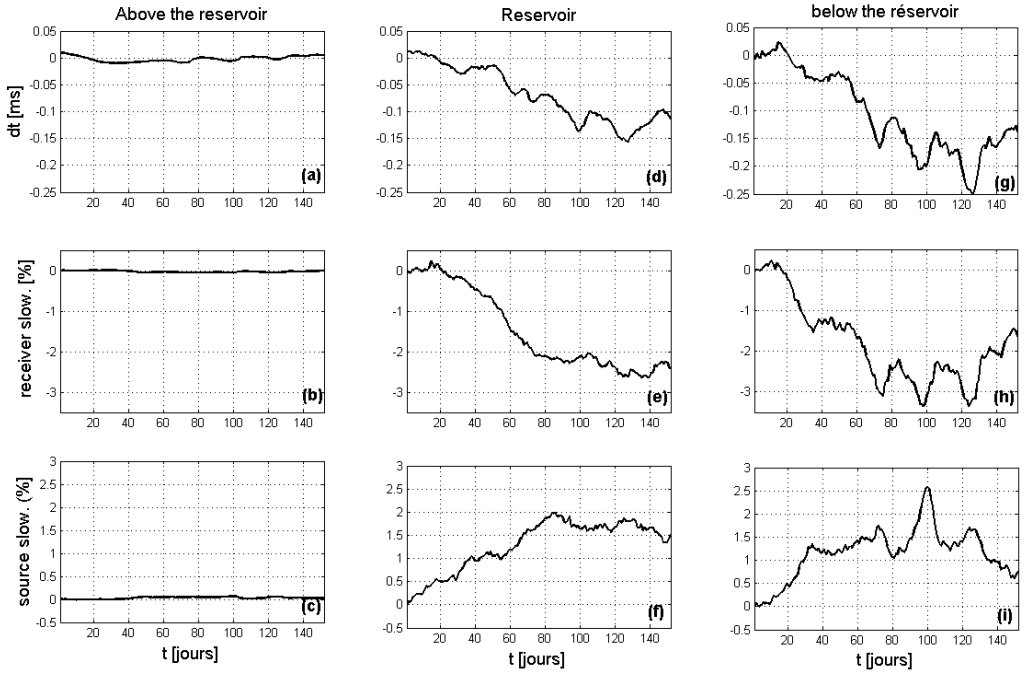

Figure 6 – (a), (d) and (g) Arrival time variations for waves 1, 2 and 3, (b), (e) and (h) Source slowness variations for waves 1, 2 and 3 and (c), (f) and (i) Receiver slowness variations for waves 1, 2 and 3.

REFERENCES

Barkved, O. I, Buer, K., Kristiansen, T. G., Kjelstadli, R. M., Kommedal, J. H., 2005, Permanent seismic monitoring at the Valhall field, Norway, Presented at the International Petroleum Technology Conference 10902-MS.

Brenguier, F., Shapiro N. M., Campillo M., Ferrazzini, V., Duputel, Z., Coutant, O. and Nercessian, A., 2008, Towards forecasting volcanic eruptions using seismic noise: Nature Geoscience. **1**, 126-130.

J. Cotton, E. Forgues, J.C. Hornman, 2012, Land Seismic Reservoir Monitoring: Where is the steam going? 82th Annual International Meeting, SEG, Expanded abstracts

David, D., Kelly, E.J. andFilson,J.R. 1971, Vespa process for analysis of seismic signals: Nature Physical Science, **232**, 8-13, 1971.

de Cacqueray, B., Roux, P., Campillo M., Catheline S. and Boue P., 2011, Elastic-wave identification and extraction through array processing: An experimental investigation at the laboratory scale: Journal of Applied Geophysics. **74**, 81-88. doi: 10.1016/j.jappgeo.2011.04.005.

de Cacqueray, B., Roux, P., Campillo, 2012, Multiple Observables 4D Monitoring and Compensation, 74th EAGE Conference and Exhibition

Forgues, E., Schissellé-Rebel, E., and Cotton, J., 2011, Simultaneous active/passive seismic monitoring of steam assisted heavy oil production; 73rd EAGE Conference and Exhibition.

Hadziioannou, C., Larose. E., Baig, A., Roux, P. and Campillo, M. 2011, Improving temporal resolution in ambient noise monitoring of seismic speed: Journal of Geophysical Research, **116**, B07304, doi:10.1029/2011JB008200.

Krüger, F., Weber, M., Scherbaum, F., and Schlittenhardt, 1996, Analysis of asymmetric multipathing with a generalization of the double-beam method: BSSA, **86**, 737-749.

C. Marandet, P. Roux, B. Nicolas, J. Mars, 2011, Target detection and localization in shallow water: an experimental demonstration of the acoustic barrier problem at the laboratory scale. Journal of Acoustical Society of America, **129**(1), 85-97.

McKay, S., Fried,J. and Carvill, C., 2003 The impact of water-velocity variations on deepwater seismic data; The Leading Edge, **22**, 344-350. doi: 10.1190/1.1572088

Meunier, J., Huguet, F., and Michel, J.M., 1997, Determining acquisition parameters time-lapse seismic recording: 59th EAGE Conference and Exhibition, Extended Abstract.

Rickett, J., and Lumley, D.E., 1998, A cross equalization processing flow for off-the-shelf 4D seismic data: 68th Annual International Meeting, SEG, Expanded Abstract.

Ross, C.P., Cunningham, G.B. and Weber, D.P., 1996, Inside the cross-equalization black box: The Leading Edge **15**, 1233-1240.

Roux P., Cornuelle, B.D., Kuperman, W.A., and Hodgkiss, W.S., 2008, The structure of raylike arrivals in a shallow-water waveguide: Journal of American Acoustic Society, **124**, 3430-3439.

Sens-Schönfelder, C. and Wegler, U., 2006, Passive image interferometry and seasonal variations of seismic velocities at Merapi Volcano, Indonesia: Geophysical Research Letters, **33**, L21302, 5 pp, doi:10.1029/2006GL027797.